Characterizing Multipartite Entanglement with Moments of Random Correlations

Andreas Ketterer,* Nikolai Wyderka, and Otfried Gühne
Naturwissenschaftlich-Technische Fakultät, Universität Siegen, Walter-Flex-Str. 3, 57068 Siegen, Germany

(Received 29 August 2018; revised manuscript received 10 December 2018; published 29 March 2019)

The experimental detection of multipartite entanglement usually requires a number of appropriately chosen local quantum measurements that are aligned with respect to a previously shared common reference frame. The latter, however, can be a challenging prerequisite, e.g., for satellite-based photonic quantum communication, making the development of alternative detection strategies desirable. One possibility for avoiding the distribution of classical reference frames is to perform a number of local measurements with settings distributed uniformly at random. In this Letter, we follow such a treatment and show that an improved detection and characterization of multipartite entanglement is possible by combining statistical moments of different order. To do so, we make use of designs that are pseudorandom processes allowing us to link the present entanglement criteria to ordinary reference frame independent ones. The strengths of our methods are illustrated in various cases, starting with two qubits and followed by more involved multipartite scenarios.

DOI: 10.1103/PhysRevLett.122.120505

Introduction.—The key role of multipartite entanglement as a resource in quantum information theory manifests itself through a variety of applications that gave rise to a growing commercial interest in quantum technologies [1–3]. Prominent examples are quantum computation or communication protocols, which have been shown to outperform known classical counterparts [3–5]. Nevertheless, its experimental detection and characterization still comes along with major technical and conceptual difficulties. One such difficulty is the alignment of local measurement settings among the involved spatially separated parties, which is a prerequisite for the evaluation of many entanglement criteria or Bell inequalities [6–8].

Several proposals that allow one to circumvent the problem of measurement alignment have been made. One is to restrict measurements to the single particle level, which has proven useful for the characterization of multipartite entanglement under the assumption that the state is pure [9,10]. Other possibilities are to encode logical qubits into rotational invariant subspaces of combined degrees of freedom [11,12], or to exploit the local-unitary (LU) invariance of entanglement criteria based on correlation functions [13–20]. The latter, commonly referred to as reference-frame (RF) independent entanglement criteria, can be evaluated without aligning spatially separated measurements [21], but they still require the experimenters' control over the choice of local measurement bases, e.g., three orthogonal ones.

Other strategies for RF independent entanglement detection lift also the last assumption in the sense that only measurements with randomly chosen settings are required. In this case, one has to resort to statistical tools that allow us to infer the entanglement properties of the considered states. For instance, in Refs. [22–24] the authors study entanglement detection given distributions of correlation functions obtained from local measurements with settings chosen uniformly at random. Similarly, one can probe the violation of Bell inequalities with randomly distributed measurement settings [25–27].

The latter attempts motivate us to push forward in this direction and to show how to considerably improve entanglement criteria based on randomly measured correlation functions [22,23]. In this Letter, we thus demonstrate that a better entanglement detection, and even a characterization of different classes of multipartite entanglement, is possible by combining statistical moments of a different order. In this respect, we will see that every such statistical entanglement criterion can be traced back to a RF independent one using pseudorandom processes, also referred to as designs. Further on, we demonstrate their strengths for the detection and characterization of multipartite entanglement involving the two lowest nonvanishing moments. We start with the instructive bipartite case of two qubits and then move to the more involved multipartite scenarios.

Moments of random correlations.—To set the stage, let us consider N qubits prepared in the initial state ρ_{in}, which are measured locally according to the random bases $\{(|u_n^{(0)}\rangle = U_n|0_n\rangle, |u_n^{(1)}\rangle = U_n|1_n\rangle)\}_{n=1,\ldots,N}$, where the $\{U_n\}_{n=1,\ldots,N}$ represent a random unitary transformation picked from the unitary group $\mathcal{U}(2)$, e.g., according to the Haar measure. We associate to the random basis $(|u_n^{(0)}\rangle = U_n|0_n\rangle, |u_n^{(1)}\rangle = U_n|1_n\rangle)$ of the nth qubit a direction $\boldsymbol{u}_n$ on the Bloch sphere, defined by the components $[\boldsymbol{u}_n]_i = \text{tr}[\sigma_{\boldsymbol{u}_n}\sigma_i]$, where σ_i, with $i = x, y, z$, denote the usual Pauli matrices and $\sigma_{\boldsymbol{u}_n} = U_n\sigma_z U_n^\dagger$ [see Fig. 1(a)]. One choice of such a set of local random measurement bases leads to the (random) correlation function:

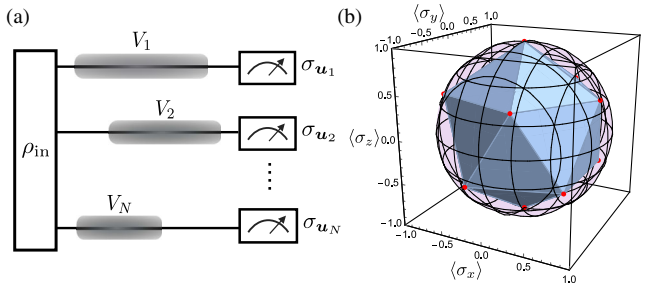

FIG. 1. (a) Schematic representation of a N-qubit entanglement detection scheme based on local measurements with randomly chosen settings $\boldsymbol{u}_1, \ldots, \boldsymbol{u}_N$. The moments $\mathcal{R}^{(t)}$ are invariant under LU transformations $\{V_n\}_{n=1,\ldots,N}$ (grey shaded areas), which might be caused by the qubits propagation, e.g., the propagation of optical qubits through fiber. (b) Plot of the 6 measurement settings corresponding to the spherical 5-design. Each direction yields two points on the Bloch sphere, which together yield the vertices of an icosahedron, i.e., a polyhedron with twenty equilateral triangular faces.

$$E(\boldsymbol{u}_1, \ldots, \boldsymbol{u}_N) = \langle \sigma_{\boldsymbol{u}_1} \otimes \ldots \otimes \sigma_{\boldsymbol{u}_N} \rangle_{\rho_{\text{in}}}. \tag{1}$$

However, as the directions $\boldsymbol{u}_n$ are chosen randomly, only one set of random measurement settings will not give any insight into the nonlocal properties of the initial state ρ_{in}. To achieve this, we have to perform several rounds of random measurements and seek a statistical treatment of the obtained values of the correlation function (1) through its moments. In order to predict the outcome of this approach, we assume that the local measurement directions $\{\boldsymbol{u}_n\}_{n=1,\ldots,N}$ are chosen uniformly from the Bloch sphere corresponding to Haar random unitaries $\{U_n\}_{n=1,\ldots,N}$. In this scenario the corresponding moments read:

$$\mathcal{R}^{(t)} = \frac{1}{(4\pi)^N} \int_{S^2} d\boldsymbol{u}_1 \ldots \int_{S^2} d\boldsymbol{u}_N E(\boldsymbol{u}_1, \ldots, \boldsymbol{u}_N)^t, \tag{2}$$

where t is a positive integer and $d\boldsymbol{u}_i = \sin\theta_i d\theta_i d\phi_i$ denotes the uniform measure on the Bloch sphere S^2. As the integrals in Eq. (2) can be rewritten in terms of integrals with respect to Haar measures on $\mathcal{U}(2)$, the moments $\mathcal{R}^{(t)}$ are by definition LU invariant and thus good candidates for RF independent entanglement detection. Also, due to the symmetry of the correlation functions (1), we can already conclude that $\mathcal{R}^{(t)} = 0$, for all odd t {also see the Supplemental Material (SM) [28]}.

Moments from designs.—In order to evaluate the uniform averages over the Bloch sphere in Eq. (2) we can resort to so-called spherical t designs, which consist of a finite set of points $\{\boldsymbol{u}_k \in S^2 | k = 1, \ldots, L^{(t)}\} \subset S^2$ fulfilling the property

$$\frac{1}{L^{(t)}} \sum_{k=1}^{L^{(t)}} P_t(\boldsymbol{u}_k) = \int_{S^2} d\boldsymbol{u} P_t(\boldsymbol{u}), \tag{3}$$

for all homogeneous polynomials $P_t\colon S^2 \to \mathbb{R}$ of degree at most t [32]. As $E(\boldsymbol{u}_1, \ldots, \boldsymbol{u}_N)^t$ is such a polynomial in each of its local settings $\boldsymbol{u}_k$, Eq. (3) directly yields the formula:

$$\mathcal{R}^{(t)} = \frac{1}{(L^{(t)})^N} \sum_{k_1,\ldots,k_N=1}^{L^{(t)}} E(\boldsymbol{u}_{k_1}, \ldots, \boldsymbol{u}_{k_N})^t, \tag{4}$$

where $\{\boldsymbol{u}_{k_j} | k_j = 1, \ldots, L^{(t)}\}$, for all j, are spherical t designs. Hence, we find as a first result that spherical t designs allow for an evaluation of the $\mathcal{R}^{(t)}$'s based on a finite number $L^{(t)}$ of local measurement settings and thus directly link them to RF independent entanglement criteria [13–20]. Furthermore, we note that similar implications also hold for systems of larger local dimensions where one has to resort to unitary designs for the evaluation of the respective moments [33–37] (see also SM [28] for more details).

The drawback of spherical and unitary designs is that, while their existence has been proven [32], there is no general strategy known to construct them for a given t. Nonetheless, by exploiting group theoretical methods it was possible to find a number of examples of exact spherical [38] and unitary designs [34]. For instance, a well-known example is the Clifford group which forms a unitary 3-design and, for a qubit, reduces to a spherical 3-design on the Bloch sphere consisting of $L^{(3)} = 6$ orthogonal directions $\{\pm\boldsymbol{e}_i | i = x, y, z\}$. Furthermore, a number of finite rotation groups on the Bloch sphere were identified as spherical designs of order $t \leq 20$ [38]. An example of such a spherical design, with $t = 5$, is given by the vertices $\{\boldsymbol{v}_i | i = 1, \ldots, L^{(5)} = 12\}$, forming the polyhedron presented in Fig. 1(b). Hence, following Eq. (4), we find

$$\mathcal{R}^{(2)} = \frac{1}{3^N} \sum_{i_1,\ldots,i_N=x,y,z} E(\boldsymbol{e}_{i_1}, \ldots, \boldsymbol{e}_{i_N})^2, \tag{5}$$

$$\mathcal{R}^{(4)} = \frac{1}{6^N} \sum_{i_1,\ldots,i_N=1}^{6} E(\boldsymbol{v}_{i_1}, \ldots, \boldsymbol{v}_{i_N})^4, \tag{6}$$

where the limits, $L^{(3)}/2 = 3$ and $L^{(5)}/2 = 6$, respectively, are halved due to the symmetry of Eq. (1). Equations (5) and (6) thus manifest the growth of measurement settings that are required for the evaluation of moments with increasing order, a fact that also yields interesting prospects for generalizations of spin-squeezing inequalities [39–42]. Lastly, note that in a similar manner one can obtain expressions for higher moments, but for the remainder of the paper we will mainly focus on $\mathcal{R}^{(2)}$ and $\mathcal{R}^{(4)}$.

Bipartite entanglement.—An important subclass of two-qubit states is that of Bell diagonal (BD) states, which are defined as $\rho_{\text{BD}} = \frac{1}{4}[\mathbb{1}_4 + \sum_{j=x,y,z} c_j \sigma_j \otimes \sigma_j]$, with real parameters c_j, such that $0 \leq |c_j| \leq 1$, and the eigenvalues λ_j of ρ_{BD} are given by $\lambda_{1,2} = (1 \mp c_1 \mp c_2 - c_3)/4$ and $\lambda_{3,4} = (1 \pm c_1 \mp c_2 + c_3)/4$ [43]. In Fig. 2 we present the

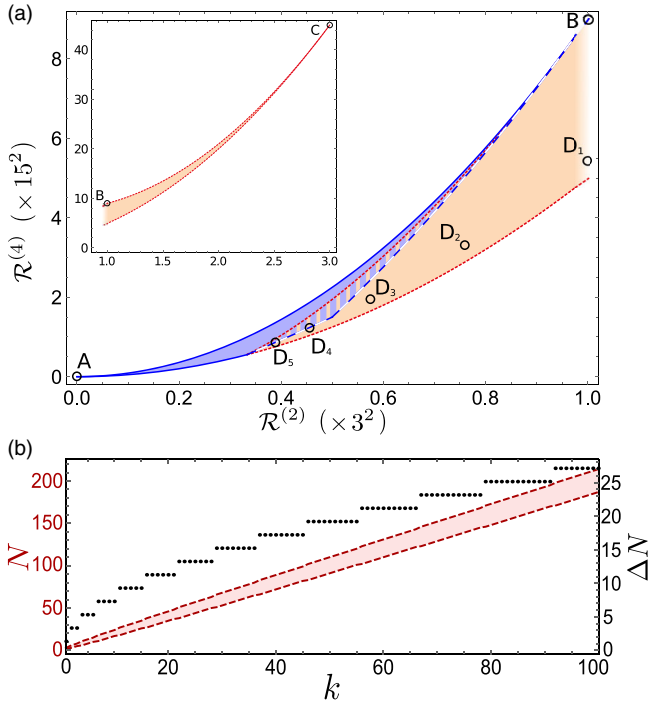

FIG. 2. (a) Representation of the set of two-qubit separable (blue solid lines) and entangled (red dotted lines) BD states in the space spanned by the moments $\mathcal{R}^{(2)}$ and $\mathcal{R}^{(4)}$ in the range $0 \leq \mathcal{R}^{(2)} \leq 1/3^2$. For $\mathcal{R}^{(2)} \leq 1/3^3$ all states are separable, and for $1/3^3 \leq \mathcal{R}^{(2)} \leq 1/3^2$, separable and entangled states have a nonzero overlap (striped region). The two-qubit criterion discussed in the main text is indicated by the white dashed curve. The inset depicts the rest of the set of entangled states in the range $1/3^2 \leq \mathcal{R}^{(2)} \leq 1/3$. The maximally mixed state (A), the pure product states (B) and the Bell states (C) are indicated by labeled black circles. Circles labeled (D_1) to (D_5) represent Dicke reduced states $|D^N_{k=2}\rangle$, with $N = 3, \ldots, 7$. (b) Dicke states $|D^N_k\rangle$ detected from two-body correlations. The red area represents values of N and k for which the criterion (7) is violated. Black dots show the range $\Delta N = N_{\max} - N_{\min}$, where $N_{\max}$ and $N_{\min}$ indicate the piecewise parallel upper and lower bounds of the red area, as a function of k.

set of BD states in the space spanned by the moments $\mathcal{R}^{(2)}$ and $\mathcal{R}^{(4)}$, obtained from an analytic optimization over the parameters c_1, c_2, and c_3 (for details see the SM [28]). In the same figure we indicate the division of the set of states into an separable and entangled part, as it results from the separability condition $|c_1| + |c_2| + |c_3| \leq 1$. Note that, there remains a small overlap between the two sets containing both separable and entangled BD states that can be distinguished perfectly by taking into account also the moment $\mathcal{R}^{(6)}$, as shown in the SM [28]. Hence, the entanglement of Bell diagonal states is completely characterized by the first three nonvanishing moments $\mathcal{R}^{(t)}$, with $t = 2, 4, 6$.

Further on, we note that for any general two-qubit state ρ one can find a BD state ρ_{BD} that has the same moments. This is a direct consequence of the fact that the $\mathcal{R}^{(t)}$'s are LU invariant, and that the transformation eliminating the local Bloch vector components of ρ is separable. In conclusion, the set of general and BD states are identical in the space spanned by the moments (see Fig. 2). Furthermore, as separable transformations are entanglement nonincreasing, we obtain our main result: for separable states, one has

$$F(\mathcal{R}^{(2)}, \mathcal{R}^{(4)}) \geq 0, \tag{7}$$

where F is a piecewise polynomial function characterizing the border of the separable set, derived in the SM [28]. It is evident that (7) detects more entangled states than any criteria, depending only on either of the moments: $\mathcal{R}^{(2)} \leq 1/3^2$ [13,22] or $\mathcal{R}^{(4)} \leq 1/5^2$ [28].

Multiqubit entanglement.—As application of the above bipartite criterion for the detection of multiqubit entanglement, we consider the class of Dicke states which for N qubits read $|D^N_k\rangle = 1/\sqrt{\binom{N}{k}} \sum_j P_j (|1\rangle^{\otimes k} |0\rangle^{\otimes (N-k)})$, where k is the number of excitations and $\sum_j P_j$ denotes the sum over all nonequivalent permutations among the qubits. As Dicke states are invariant under permutations of their subsystems, we can detect their entanglement by focusing on any of their two-qubit marginals. We also emphasize that none of the states $|D^N_k\rangle$, for any N and k, can be detected using only either of the moments $\mathcal{R}^{(2)}$ or $\mathcal{R}^{(4)}$. In contrast, our novel nonlinear criterion (7) is capable detecting Dicke state entanglement. For instance, in the case of the N-qubit W-state $|W_N\rangle = |D^N_{k=1}\rangle$ we can ascertain entanglement for $N \leq 3$. The same holds for a subset of Dicke states with $k > 1$. In Fig. 2(b), we represent the set of Dicke states detected by our criterion for up to 200 qubits.

In order to obtain better criteria that are capable of detecting more entangled states, we have to take into account moments of N-body correlation functions. In this respect, we note that entanglement criteria based only on the second moment have been subject of investigations in the context of correlation tensor norms [13–20,22]. For instance, it is known that $\mathcal{R}^{(2)} \leq 1/3^N$ for all separable N-qubit states. Here, we ask whether these results can be improved upon by combining N-body moments of different order. However, an analytical characterization of the borders of the set of (separable) states as presented for two qubits becomes very demanding already for three parties. Despite this difficulty, we gained insight into the structure of the three-qubit state space by numerically generating more than 10^5 random (fully separable) states. In Fig. 3(a) we present the results of this procedure. As for two qubits, we find that an advantage for entanglement detection is possible by taking into account $\mathcal{R}^{(4)}$. An analytical proof of this observation, in particular for more qubits, remains subject of future investigations.

Classes of multipartite entanglement.—In the multipartite case, it is also of interest to discriminate different classes of multipartite entanglement that are defined through the concept of stochastic local operations and classical communication (SLOCC) [44,45]. Two pure N-qubit states $|\Psi\rangle$ and $|\Phi\rangle$ are SLOCC equivalent if there exist invertible operations A_i, with $i = 1, \ldots, N$, such that $|\Psi\rangle = \bigotimes_{i=1}^{N} A_i |\Phi\rangle$. The corresponding equivalence classes that result from this definition are referred to as SLOCC classes. While for three parties there exist two SLOCC classes of genuinely multipartite entangled states, the W- and the GHZ-class [44], they become infinitely many already for $N = 4$ [46]. In the following, we will concentrate our attention on the corresponding equivalence classes of N qubits, referred to as $\mathcal{W}^{(N)}$ and $\mathcal{GHZ}^{(N)}$. As for separable states the respective sets of mixed states are given by the convex hulls $\mathrm{Conv}(\mathcal{W}^{(N)})$ and $\mathrm{Conv}(\mathcal{GHZ}^{(N)})$ [45].

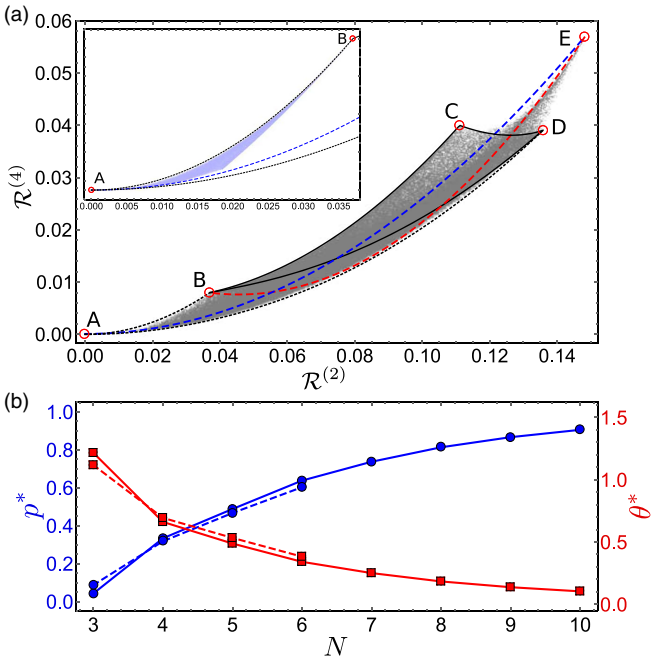

FIG. 3. (a) Representation of the set of three-qubit states in the space spanned by the moments $\mathcal{R}^{(2)}$ and $\mathcal{R}^{(4)}$. Gray points correspond to randomly generated mixed quantum states. Labeled red circles indicate the maximally mixed state (A), all pure product states (B), biseparable states of the form $|\phi\rangle|\mathrm{Bell}\rangle$ (C), the three-qubit W- (D), and the GHZ-state (E). While the black lines connecting (B), (C), and (D) enclose the set $\mathcal{W}^{(3)}$, its mixed extension $\mathrm{Conv}(\mathcal{W}^{(3)})$ is indicated by black dotted lines. The noisy GHZ state (blue dashed line) and the pure state $|\Psi(\theta)\rangle$ (red dashed-dotted line) are shown for $0 \le p \le 1$ and $0 \le \theta \le \pi/2$, respectively. The inset shows randomly generated fully separable states (light blue points) in the range $0 \le \mathcal{R}^{(2)} \le 1/3^3$. (b) Plot of the noise threshold p^* (blue dots, left scale) up to which a GHZ state is detected to be not in $\mathrm{Conv}(\mathcal{W}^{(N)})$. Solid and dashed lines refer to thresholds obtained from the criteria $\mathcal{R}^{(2)} \le \chi^{(N)}$ and $m^{(N)}\mathcal{R}^{(2)} + \tilde{b}^{(N)} \ge \mathcal{R}^{(4)}$, respectively, for varying number of qubits N. Accordingly, red squares show the amplitude threshold θ^* (red right scale) above which $|\Psi(\theta)\rangle$ is detected to be outside of $\mathcal{W}^{(N)}$.

For the characterization of the W-class, it is helpful to resort to its standard form representing all pure W-class states up to LU transformations [47–49]. The latter allows us to numerically determine the borders of the pure W-class in the space spanned by the moments $\mathcal{R}^{(t)}$, as presented in Fig. 3(a), for $N = 3$. In the same figure we present an estimate of the borders of the mixed W-class which has been obtained by minimizing over a subclass of $\mathrm{Conv}(\mathcal{W}^{(N)})$ and confirmed by generating more than 10^5 mixed W-class states (for details of this procedure see the SM [28]). As a result, we see that a discrimination of states outside of the W-class based on the knowledge of $\mathcal{R}^{(2)}$ and $\mathcal{R}^{(4)}$ is possible.

With increasing qubit number, the numerical characterization of the complete W-class becomes computationally more demanding. For this reason, we aim for simpler criteria that can be extended to larger numbers of qubits. One way of doing so is to compute the maximum of $\mathcal{R}^{(2)}$ in $\mathcal{W}^{(N)}$, and use its convexity to derive the criterion $\mathcal{R}^{(2)} \le \max_{\rho' \in \mathcal{W}^{(N)}} \mathcal{R}^{(2)} =: \chi^{(N)}$, for all $\rho \in \mathrm{Conv}(\mathcal{W}^{(N)})$. We further test this criterion by applying it to the noisy GHZ state $p\mathbb{1}/2^N + (1-p)|\mathrm{GHZ}\rangle\langle\mathrm{GHZ}|$ and a pure entangled state $|\Psi(\theta)\rangle = \cos\theta|0\rangle^{\otimes N} + \sin\theta|1\rangle^{\otimes N}$, and we determine the corresponding noise and amplitude thresholds, p^* and θ^*, respectively, up to which the states can be certified to be not in $\mathrm{Conv}(\mathcal{W}^{(N)})$ [see Fig. 3(b)]. Clearly, the performance of the criterion improves with growing qubit number.

Lastly, we take an attempt to go beyond these results through a more general criterion that combines $\mathcal{R}^{(2)}$ and $\mathcal{R}^{(4)}$. Examining the structure of the W-class in Fig. 3(a), we expect that a line passing through the points C and D yields such an improvement. For an arbitrary N, such a line can be derived by first maximizing individually, $\mathcal{R}^{(2)}$ and $\mathcal{R}^{(4)}$, over $\mathcal{W}^{(N)}$. The resulting arguments of these maximizations then allow us to define a line with slope $m^{(N)}$. Second, we maximize the $\mathcal{R}^{(4)}$-intercept $b^{(N)}$ of this line over $\mathcal{W}^{(N)}$ to ensure that it touches its border. Finally, as a linear combination of two convex functions with positive coefficients is again convex, we arrive at the criterion $m^{(N)}\mathcal{R}^{(2)} + \tilde{b}^{(N)} \ge \mathcal{R}^{(4)}$, for all $\rho \in \mathrm{Conv}(\mathcal{W}^{(N)})$ and with $\tilde{b}^{(N)} = \max_{\rho \in \mathcal{W}^{(N)}} b^{(N)}$, as demonstrated in the SM [28]. The performance of the latter is presented Fig. 3(b). Evidently, the observed improvement for three qubits does not hold for a larger qubit number. Hence, in order to improve the above results, a more refined nonlinear witness is desirable.

Experimental considerations.—The discussed methods are of interest for photonic free-space quantum communication over distances of several hundreds of kilometers [50],

which is currently in the process of being extended to space involving satellites orbiting the earth [51–54]. Here, due to the motion, distance, and number of involved satellites, the issue of sharing classical reference frames becomes particularly challenging [10–12]. In such a scenario, the moments (2) can either be evaluated exactly through the fixed measurement settings involved in Eqs. (5) and (6), in the spirit of RF independent entanglement criteria [19]. Alternatively, they can be estimated using a statistical treatment based on a finite number of randomly chosen settings. The latter can be achieved experimentally by digitally generating random unitary transformations that are subsequently applied prior to the photon polarization measurements (see, e.g., Ref. [55]). Also note that, according to the analysis presented in Refs. [22,23], the number of random measurement settings needed to certify entanglement with confidence scales favorably with the system size, thus making it an attractive method in the multipartite regime.

Conclusions.—A major challenge for the experimental detection and characterization of multipartite entanglement is the need of sharing a common RF allowing us to coordinate measurements taken at a distance. In this Letter, we showed how to considerably improve existing techniques for RF independent entanglement verification by combining statistical moments of correlation functions obtained from measurements taken with randomly distributed settings. To this effect, we made use of designs that allow for a straightforward evaluation of the corresponding moments. We demonstrated the introduced techniques by applying them to detect entanglement in multiqubit systems and also to discriminate different classes of multipartite entanglement.

Finally, our results yield interesting prospects for generalizations of the spin-squeezing inequalities derived in Refs. [39–42] and the entanglement criteria obtained in Refs. [56,57]. Although such generalized criteria would lose the LU invariance property, the extension of the number of local measurement settings originating from the spherical 5-design is expected to entail an improvement in their detection power.

We appreciate helpful comments by H. Chau Nguyen on this work, and we thank Nicolas Brunner, Marcus Huber, Lukas Knips, Daniel McNulty, Jasmin Meinecke, Tomasz Paterek, Gael Sentís, Timo Simnacher, Cornelia Spee, and Xiao-Dong Yu for fruitful discussions. We acknowledge financial support from the ERC (Consolidator Grant No. 683107/TempoQ) and the DFG. N. W. acknowledges support from the House of Young Talents Siegen.

*Present address: Physikalisches Institut, Albert-Ludwigs-Universität Freiburg, Hermann-Herder-Str. 3, 79104 Freiburg, Germany.

[1] R. Horodecki, P. Horodecki, M. Horodecki, and K. Horodecki, Rev. Mod. Phys. **81**, 865 (2009).
[2] A. Acín, I. Bloch, H. Buhrman, T. Calarco, C. Eichler, J. Eisert, D. Esteve, N. Gisin, S. J. Glaser, F. Jelezko, S. Kuhr, M. Lewenstein, M. F. Riedel, P. O. Schmidt, R. Thew, A. Wallraff, I. Walmsley, and F. K. Wilhelm, New J. Phys. **20**, 080201 (2018).
[3] M. A. Nielsen and I. L. Chuang, *Quantum Computation and Quantum Information* (Cambridge University Press, New York, 2000).
[4] S. Pirandola, J. Eisert, C. Weedbrook, A. Furusawa, and S. L. Braunstein, Nat. Photonics **9**, 641 (2015).
[5] N. Gisin, G. Ribordy, W. Tittel, and H. Zbinden, Rev. Mod. Phys. **74**, 145 (2002).
[6] O. Gühne and G. Tóth, Phys. Rep. **474**, 1 (2009).
[7] J. S. Bell, Physics **1**, 195 (1964).
[8] N. Brunner, D. Cavalcanti, S. Pironio, V. Scarani, and S. Wehner, Rev. Mod. Phys. **86**, 419 (2014).
[9] M. Walter, B. Doran, D. Gross, and M. Christandl, Science **340**, 1205 (2013).
[10] G. H. Aguilar, S. P. Walborn, P. H. Souto Ribeiro, and L. C. Céleri, Phys. Rev. X **5**, 031042 (2015).
[11] L. Aolita and S. P. Walborn, Phys. Rev. Lett. **98**, 100501 (2007).
[12] V. D'Ambrosio, E. Nagali, S. P. Walborn, L. Aolita, S. Slussarenko, L. Marrucci, and F. Sciarrino, Nat. Commun. **3**, 961 (2012).
[13] H. Aschauer, J. Calsamiglia, M. Hein, and H. J. Briegel, Quantum Inf. Comput. **4**, 383 (2004).
[14] J. I. de Vicente, Quantum Inf. Comput. **7**, 624 (2007).
[15] J. I. de Vicente, J. Phys. A **41**, 065309 (2008).
[16] J. I. de Vicente and M. Huber, Phys. Rev. A **84**, 062306 (2011).
[17] P. Badziag, C. Brukner, W. Laskowski, T. Paterek, and M. Żukowski, Phys. Rev. Lett. **100**, 140403 (2008).
[18] W. Laskowski, M. Markiewicz, T. Paterek, and M. Żukowski, Phys. Rev. A **84**, 062305 (2011).
[19] T. Lawson, A. Pappa, B. Bourdoncle, I. Kerenidis, D. Markham, and E. Diamanti, Phys. Rev. A **90**, 042336 (2014).
[20] C. Klöckl and M. Huber, Phys. Rev. A **91**, 042339 (2015).
[21] S. D. Bartlett, T. Rudolph, and R. W. Spekkens, Rev. Mod. Phys. **79**, 555 (2007).
[22] M. C. Tran, B. Dakić, F. Arnault, W. Laskowski, and T. Paterek, Phys. Rev. A **92**, 050301(R) (2015).
[23] M. C. Tran, B. Dakić, W. Laskowski, and T. Paterek, Phys. Rev. A **94**, 042302 (2016).
[24] A. Gabriel, Ł. Rudnicki, and B. C. Hiesmayr, New J. Phys. **15**, 073033 (2013).
[25] Y.-C. Liang, N. Harrigan, S. D. Bartlett, and T. Rudolph, Phys. Rev. Lett. **104**, 050401 (2010).
[26] P. Shadbolt, T. Vértesi, Y.-C. Liang, C. Branciard, N. Brunner, and J. L. O'Brien, Sci. Rep. **2**, 470 (2012).
[27] C. Furkan Senel, T. Lawson, M. Kaplan, D. Markham, and E. Diamanti, Phys. Rev. A **91**, 052118 (2015).
[28] See Supplemental Material at http://link.aps.org/supplemental/10.1103/PhysRevLett.122.120505 for the appendices which also refer to Refs. [29–31].
[29] X. Zheng-Jun, X. Heng-Na, L. Yong-Ming, and W. Xiao-Guang, Commun. Theor. Phys. **57**, 771 (2012).
[30] Z. Webb, Quantum Inf. Comput. **16**, 1379 (2016).

[31] H. Zhu, R. Kueng, M. Grassl, and D. Gross, arXiv: 1609.08172.
[32] P. D. Seymour and T. Zaslavsky, Adv. Math. **52**, 213 (1984).
[33] C. Dankert, M.Sc. thesis, University of Waterloo, 2005; also available as e-print, arXiv:quant-ph/0512217.
[34] D. Gross, K. Audenaert, and J. Eisert, J. Math. Phys. (N.Y.) **48**, 052104 (2007).
[35] F. G. S. L. Brandão, A. W. Harrow, and M. Horodecki, Phys. Rev. Lett. **116**, 170502 (2016).
[36] F. G. S. L. Brandão, A. W. Harrow, and M. Horodecki, Commun. Math. Phys. **346**, 397 (2016).
[37] Y. Nakata, C. Hirche, M. Koashi, and A. Winter, Phys. Rev. X **7**, 021006 (2017).
[38] R. H. Hardin and N. J. A. Sloane, Discrete Comput. Geom. **15**, 429 (1996).
[39] G. Toth, C. Knapp, O. Gühne, and H. J. Briegel, Phys. Rev. Lett. **99**, 250405 (2007).
[40] D. J. Wineland, J. J. Bollinger, W. M. Itano, and D. J. Heinzen, Phys. Rev. A **50**, 67 (1994).
[41] A. Sørensen and K. Mølmer, Phys. Rev. Lett. **83**, 2274 (1999).
[42] A. Sørensen, L.-M. Duan, J. I. Cirac, and P. Zoller, Nature (London) **409**, 63 (2001).
[43] R. Horodecki and M. Horodecki, Phys. Rev. A **54**, 1838 (1996).
[44] W. Dür, G. Vidal, and J. I. Cirac, Phys. Rev. A **62**, 062314 (2000).
[45] A. Acín, D. Bruß, M. Lewenstein, and A. Sanpera, Phys. Rev. Lett. **87**, 040401 (2001).
[46] C. Spee, J. I. de Vicente, and B. Kraus, J. Math. Phys. (N.Y.) **57**, 052201 (2016).
[47] A. Acín, A. Andrianov, L. Costa, E. Jané, J. I. Latorre, and R. Tarrach, Phys. Rev. Lett. **85**, 1560 (2000).
[48] H. A. Carteret, A. Higuchi, and A. Sudbery, J. Math. Phys. (N.Y.) **41**, 7932 (2000).
[49] S. Kıntaş and S. Turgut, J. Math. Phys. (N.Y.) **51**, 092202 (2010).
[50] R. Ursin *et al.*, Nat. Phys. **3**, 481 (2007).
[51] J. G. Rarity, P. R. Tapster, P. M. Gorman, and P. Knight, New J. Phys. **4**, 82 (2002).
[52] M. Aspelmeyer *et al.*, Science **301**, 621 (2003).
[53] P. Villoresi *et al.*, New J. Phys. **10**, 033038 (2008).
[54] C. Bonato, A. Tomaello, V. Da Deppo, G. Naletto, and P. Villoresi, New J. Phys. **11**, 045017 (2009).
[55] M. Bourennane, M. Eibl, S. Gaertner, C. Kurtsiefer, A. Cabello, and H. Weinfurter, Phys. Rev. Lett. **92**, 107901 (2004).
[56] A. Kalev and J. Bae, Phys. Rev. A **87**, 062314 (2013).
[57] J. Bae, D. McNulty, and B. Hiesmayr, New J. Phys. **21**, 013012 (2019).